

# Navigating Explanatory Multiverse Through Counterfactual Path Geometry

Kacper Sokol<sup>\*1, 2</sup>, Edward Small<sup>\*2</sup>, Yueqing Xuan<sup>\*2</sup>

<sup>1</sup>Department of Computer Science, ETH Zurich, Switzerland

<sup>2</sup>ARC Centre of Excellence for Automated Decision-Making and Society, RMIT University, Australia  
kacper.sokol@inf.ethz.ch, edward.small@student.rmit.edu.au, yueqing.xuan@student.rmit.edu.au

## Abstract

Counterfactual explanations are the de facto standard when tasked with interpreting decisions of (opaque) predictive models. Their generation is often subject to algorithmic and domain-specific constraints – such as density-based feasibility, and attribute (im)mutability or directionality of change – that aim to maximise their real-life utility. In addition to desiderata with respect to the counterfactual instance itself, existence of a viable path connecting it with the factual data point, known as algorithmic recourse, has become an important technical consideration. While both of these requirements ensure that the steps of the journey as well as its destination are admissible, current literature neglects the *multiplicity* of such counterfactual paths. To address this shortcoming we introduce the novel concept of *explanatory multiverse* that encompasses all the possible counterfactual journeys. We then show how to navigate, reason about and compare the geometry of these trajectories with two methods: vector spaces and graphs. To this end, we overview their spacial properties – such as affinity, branching, divergence and possible future convergence – and propose an all-in-one metric, called *opportunity potential*, to quantify them. Implementing this (possibly interactive) explanatory process grants explainees agency by allowing them to select counterfactuals based on the properties of the journey leading to them in addition to their absolute differences. We show the flexibility, benefit and efficacy of such an approach through examples and quantitative evaluation on the German Credit and MNIST data sets.

## 1 Multiplicity of Counterfactual Paths

Counterfactuals are the go-to explanations when faced with unintelligible machine learning (ML) models. Their appeal – both to lay and technical audiences – is grounded in decades of research in the social sciences (Miller 2019) as well as compliance with various legal frameworks (Wachter, Mittelstadt, and Russell 2017). Fundamentally, counterfactual explanation generation relies on finding an instance whose predicted class is different from that of the factual data point while minimising the distance between the two instances – a flexible retrieval process that can be tweaked to satisfy bespoke desiderata.

<sup>\*</sup>Equal contribution.

ICML (International Conference on Machine Learning) Workshop on Counterfactuals in Minds and Machines, Honolulu, Hawaii, USA. Copyright 2023 by the author(s).

The increasing popularity of counterfactuals and their highly customisable generation mechanism have spurred researchers to incorporate sophisticated technical and social requirements into their retrieval algorithms to better reflect their real-life situatedness. Relevant technical aspects include tweaking the fewest possible attributes to guarantee explanation sparsity, or ensuring that counterfactual instances come from a data manifold either by relying on hitherto observed instances (Keane and Smyth 2020; Poyiadzi et al. 2020; van Looveren and Klaise 2021) or by constructing them in dense regions (Förster et al. 2021). Desired social properties reflect real-life constraints imposed by the underlying operational context and data domain, e.g., (im)mutability of certain features, such as date of birth, and directionality of change of others, such as age. The mechanisms employed to retrieve these explanations have evolved accordingly: from techniques that simply output counterfactual instances (Wachter, Mittelstadt, and Russell 2017; Russell 2019; Romashov et al. 2022), possibly accounting for selected social and technical desiderata as part of optimisation, to methods that construct viable paths between factual and counterfactual points, referred to as *algorithmic recourse* (Ustun, Spangher, and Liu 2019; Clark et al. 2024), ensuring feasibility of this journey and actionability of the prescribed interventions (Poyiadzi et al. 2020; Downs et al. 2020; Förster et al. 2021; Karimi, Schölkopf, and Valera 2021).

All of these properties aid in generating admissible counterfactuals, but they do not offer guidance on how to discriminate between them. Available explainers tend to output multiple counterfactuals whose differences, as it stands, can only be captured through: high-level desiderata, e.g., chronology and coherence; quantitative metrics, e.g., completeness, proximity and neighbourhood density; or qualitative assessment, e.g., user trust and confidence (Sokol and Flach 2020a; Keane et al. 2021; Small et al. 2023; Xuan et al. 2023; Sokol and Vogt 2024). In principle, explanation plurality is desirable since it facilitates (interactive) personalisation by offering versatile sets of actions to be taken by the explainees instead of just the most optimal collection of steps (according to a predefined objective), thus catering to unique needs and expectations of diverse audiences (Sokol and Flach 2018, 2020c). Nonetheless, this multiplicity is also problematic as without incorporating domain-specific knowledge, collect-

ing user input or relying on generic “goodness” heuristics and criteria to filter out redundant explanations – which aspects remain open challenges in themselves – they are likely to overwhelm the explainees (Keane et al. 2021).

While comparing counterfactual instances based on their diversity as well as overall feasibility and actionability, among other properties, may inform their pruning, considering the (geometric) relation between the paths leading to them could prove more potent. Current literature treats counterfactual explanations as *independent* and disregards both their lineage as well as the process that transforms a factual data point into a counterfactual instance, which may unravel over an extended time period (Barocas, Selbst, and Raghavan 2020; Verma et al. 2020). The *spatial relation* between counterfactual paths is also overlooked, whether captured by their direction, length or number of discrete steps (including alignment and size thereof). Additionally, while the feasibility of attribute tweaks, i.e., feature actionability or mutability, is often considered, the direction and magnitude of such changes is largely neglected, e.g., age can only increase at a fixed rate. Modelling such aspects of counterfactual paths is bound to offer domain-independent, spatially-informed heuristics that reduce the number of explanations for users to consider, grant them agency, inform their decision-making and support reasoning as well as forward planning.

The role of geometry in (counterfactual) explainability is captured by Figure 1, which demonstrates the diverse characteristics of counterfactual paths for a two-dimensional toy data set with continuous numerical features. When considered in *isolation*, these paths have the following properties:

- A** is short and leads to a high-confidence region, but it lacks data along its journey, which signals infeasibility;
- B** while shorter, it terminates close to a decision boundary, thus carries high uncertainty;
- C** addresses the shortcomings of A, but it lands in an area of high instability (compared to D,  $E_i$ , F, G & H);
- G & H** also do not exhibit the deficiencies of A, but they are located in a region with a high error rate;
- D & F** have all the desired properties, but they are the most distant; and
- $E_i$  are feasible, but they are *incomplete* by themselves.

While such considerations have become commonplace in the literature, they treat each destination and path leading to it independently, thus forgoing the benefit of accounting for their spatial relation such as affinity, branching, divergence or convergence. For example, accessing D, F & G via  $E_i$  elongates the journey leading to these counterfactuals, making them less attractive based on current desiderata; nonetheless, such a path maximises the agency of explainees by providing them with multiple recourse choices along a *unified* trajectory.

Reasoning about the properties of and comparing counterfactual paths is intuitive in two-dimensional spaces – as demonstrated by Figure 1 – but doing so in higher dimensions requires a more principled approach. To this end, we formalise the concept of *explanatory multiverse*, which embraces the multiplicity of counterfactual explanations and

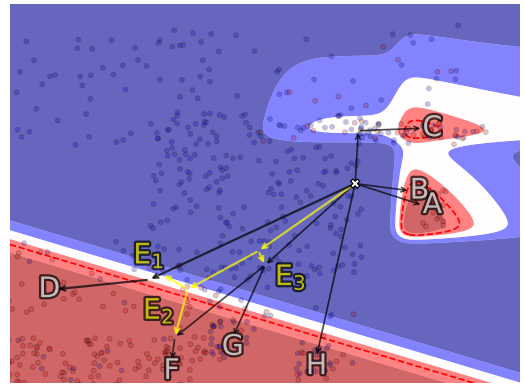


Figure 1: Example of *explanatory multiverse* constructed for tabular data with two continuous (numerical) features. It demonstrates various types of *counterfactual path geometry*: their *affinity*, *branching*, *divergence* and *convergence*. Each journey terminates in a (possibly the same or similar) counterfactual explanation but the characteristics of the steps leading there make some explanations more attractive targets, e.g., by giving the explainee more agency through multiple actionable choices towards the end of a path.

captures the *geometry*, i.e., spatial dependence, of journeys leading to them, and position it in the current literature (Section 2). Our conceptualisation accounts for technical, *spatially-unaware* desiderata prevalent in the literature – e.g., plausibility, path length, number of steps, sparsity, magnitude of attribute change and feature actionability – and defines novel, *spatially-aware* properties such as branching delay, branching factor, (change in) path directionality and affinity between journeys. We then propose two implementations of explanatory multiverse:

1. vector-based paths, which can rely on data density (model-agnostic) or gradient methods, and are apt for predominantly continuous feature spaces (Section 3); and
2. pathfinding in (directed) graphs, which can be built for data based on a predefined distance metric, and is best suited for mostly discrete feature spaces (Section 4).

In addition to imbuing counterfactuals with spatial awareness, explanatory multiverse reduces the number of admissible explanations by *collapsing* paths based on their affinity and *pruning* them through our spatially-aware desiderata. To quantify these properties we formalise an all-in-one metric, called *opportunity potential*, for each realisation of explanatory multiverse. Experiments on the German Credit (Hofmann 1994) and MNIST (LeCun 1998) data sets (Section 5) demonstrate the flexibility, benefit and efficacy of our approach through examples and numerical evaluation. We invite others to embark on this novel counterfactual explainability research journey by releasing a Python package, called FACELIFT<sup>1</sup>, that implements our methods.

From the explainees’ perspective, our approach helps them to navigate explanatory multiverse and grants them initiative and agency, empowering meaningful exploration,

<sup>1</sup><https://github.com/xuanxuanxuan-git/facelift>

customisation and personalisation of counterfactuals. For example, by choosing a path recommended based on a high number of diverse explanations accessible along it – refer to segments  $E_i$  in Figure 1, which have high opportunity potential – the user is given ample chance to receive the desired outcome while applying a consistent set of changes, thus reducing the number of u-turns and backtracking arising in the process. Explanatory multiverse is also compatible with human-in-the-loop, interactive explainability (Sokol and Flach 2018, 2020c; Keenan and Sokol 2023) and a relatively recent decision-support model of explainability, which relies on co-construction of explanations and complements the more ubiquitous “prediction justification” paradigm (Miller 2023). We explore and discuss these concepts further in Section 6, before concluding the paper and outlining future work in Section 7.

## 2 Preliminaries

Before we formalise explanatory multiverse desiderata (Section 2.3), we position this concept in the current literature (Section 2.1) and summarise the notation (Section 2.2) used to introduce our two methods. Throughout this paper we assume that we are given a (state-of-the-art) explainer that generates counterfactuals along with steps leading to them, such as FACE (Poyiadzi et al. 2020) or any other algorithmic recourse technique (Ustun, Spangher, and Liu 2019; Karimi, Schölkopf, and Valera 2021). Our methods work with explainers that follow actual data instances and those that operate directly on feature spaces (e.g., relying on data distribution density).

### 2.1 Related Work

Existing counterfactual explainers account for multiple desiderata pertaining to the counterfactual instances themselves – i.e., *spatially-unaware* properties – to ensure their real-life practicality. The most common requirement concerns the *distance* between the factual and counterfactual instances as well as the number of features being tweaked, striving for the smallest possible distance and number of affected attributes (Wachter, Mittelstadt, and Russell 2017; Tolomei et al. 2017). Another desideratum accounts for (domain-specific) constraints with respect to feature alterations, specifically (*im*)*mutability* of attributes, direction and rate of their change as well as their *actionability* from a user’s perspective; e.g., some tweaks are irreversible, some can be implemented by explainees and others – mutable but non-actionable – are properties of the environment (Ustun, Spangher, and Liu 2019; Karimi, Schölkopf, and Valera 2021). *Plausibility* of the counterfactual data point is also considered. It requires the explanations to be: (1) feasible according to the underlying data distribution, thus come from the data manifold, enforced either through density constraints or by following pre-existing instances; and (2) of *high confidence*, i.e., robust, in view of the explained predictive model (Pawelczyk, Broelemann, and Kasneci 2020; Poyiadzi et al. 2020; Downs et al. 2020; van Looveren and Klaise 2021). The *multiplicity* of admissible counterfactual explanations is their least explored property; explainers

should aim to output a comprehensive subset of instances that are the *most diverse*, *least similar* as well as *highly representative* (Mothilal, Sharma, and Tan 2020; Keane et al. 2021; Laugel et al. 2023).

While important, these desiderata are only concerned with the counterfactual instances themselves, thus overlooking the properties of paths connecting them with the data points being explained. Ignoring the journey between the factual and counterfactual instances is synonymous with assuming that a user can implement such changes simultaneously and instantaneously, but in reality this process often involves multiple discrete actions spread over time (Barocas, Selbst, and Raghavan 2020). Explainers such as FACE can generate a counterfactual path as a sequence of steps based on training data points, but methods capable of outputting explanations in this format are scarce (Ramakrishnan, Lee, and Albarghouthi 2020; Kanamori et al. 2021; Verma, Hines, and Dickerson 2022). These approaches, however, treat path-based counterfactual explanations as independent – ignoring the useful information carried by their spatial relation – which gap creates a need for optimisation objectives and evaluation metrics that explicitly capture various characteristics of counterfactual paths. As a first step, counterfactual instance-based metrics can be adapted to this setting, e.g., a path length and its number of steps as well as actionability and plausibility of the intermediate instances that constitute it. Nonetheless, we still lack desiderata that capture the continuity of steps given by a counterfactual path, multiplicity thereof, and their geometrical relation. Such properties become especially important for real-life implementation of algorithmic recourse that may stretch over time, in which case a path may become infeasible part way through its enactment, e.g., due to uncontrollable factors, preventing its completion and requiring a transition to an alternative route.

### 2.2 Notation

We denote the  $m$ -dimensional input space as  $\mathcal{X}$ , with the explained (factual) instance given by  $\hat{x}$  and the explanation (counterfactual) data point by  $\tilde{x}$ . These instances are considered in relation to a predictive model  $f : \mathcal{X} \mapsto \mathcal{Y}$ , where  $\mathcal{Y}$  is the space of possible classes; therefore,  $f(\hat{x}) \neq f(\tilde{x})$  and the prediction of the former data point  $f(\hat{x}) = \hat{y} \in \mathcal{Y}$  is less desirable than that of the latter  $f(\tilde{x}) = \tilde{y} \in \mathcal{Y}$ .  $\tilde{f}$  refers to the probabilistic realisation of  $f$  that outputs the probability of the desired class. Vector  $p$ -norms, which provide a measurement of length, are defined as  $\|v\|_p = (\sum_{i=1}^n |v_i|^p)^{\frac{1}{p}}$ . Distance functions, e.g., on the input space, are denoted by  $d : \mathcal{X} \times \mathcal{X} \mapsto \mathbb{R}^+$ , where the score of 0 represents identical instances, i.e.,  $d(x_a, x_b) = 0 \implies x_a \equiv x_b$ , and the higher the score, the more different the data points are.

To discover  $\tilde{x}$  and the *steps* necessary to transform  $\hat{x}$  into this instance, we apply a state-of-the-art, path-based explainer – see Section 2.1 for the properties expected of it – that generates (multiple) counterfactuals along with their journeys. Each such explanation  $Z^{[k]}$ , where  $k$  is its index, is represented by an  $m \times n$  matrix whose  $n$  columns  $z_i^{[k]} \in \mathcal{X}$  capture the sequence of steps in the  $m$ -dimensional input space, i.e.,  $Z^{[k]} = [z_1^{[k]} \dots z_n^{[k]}]$ , such that if we start at

the factual point  $\hat{x}$ , we end at the counterfactual instance  $\check{x}$  like so:  $\check{x} = \hat{x} + \sum_{i=1}^n z_i^{[k]}$ . For the *vector-based* explanatory multiverse, each step can be discounted by a weight factor  $w_i$  that captures its properties, with the weight vector  $w = [w_1 \cdots w_n]$  adhering to the following constraints:  $\|w\|_2 = 1$  and  $w_1 \geq w_2 \geq \cdots \geq w_{n-1} \geq w_n$ .

For the *graph-based* approach, we take  $G = (V, E)$  to be a (directed) graph with vertices  $V$  and arcs (directed edges)  $E$ . Each vertex  $v_i \in V$  corresponds to a data point  $x_i \in \mathcal{X}$  in the input space, i.e.,  $v_i \equiv x_i$ ; these are connected with (directed) edges  $e_{i,j} \in E$  that leave  $v_i$  and enter  $v_j$ . Assuming that  $v_1$  represents the explained instance  $\hat{x}$ , thus the starting point of a path, and  $v_n$  is the target counterfactual data point  $\check{x}$ , thus where the journey terminates, we can identify multiple paths  $Z^{[k]}$  connecting them. Here, the columns  $z_i^{[k]}$  of the  $m \times n$  matrix  $Z^{[k]}$  representing an  $n$ -step explanatory journey store a sequence of vertices  $v_i$  along this path, i.e.,  $z_i^{[k]} \equiv v_i$ , with  $z_1^{[k]} \equiv \hat{x}$  and  $z_n^{[k]} \equiv \check{x}$ . Such a journey can alternatively be denoted by the corresponding sequence of edges  $E_{1,n} = [e_{1,2} \cdots e_{n-1,n}] \subseteq E$  that encode the properties of each transition (akin to the weights  $w_i$  used in the vector space approach).

### 2.3 Spatially-aware Desiderata

Our conceptualisation of *explanatory multiverse* builds on top of the *spatially-unaware* properties discussed in Section 2.1 – which it inherits by relying on state-of-the-art, path-based counterfactual explainers – and extends these desiderata with three novel, *spatially-aware* properties.

**Agency** captures the number of choices – leading to *diverse* counterfactuals – available to explainees as they traverse explanatory paths. High agency offers a selection of explanations and stimulates *user initiative*. It can be measured as *branching factor*, i.e., the number of paths leading to representative explanations accessible at any given step.

**Loss of Opportunity** encompasses the *incompatibility* of subsets of explanations that emerges as a consequence of implementing changes prescribed by steps along a counterfactual path. For example, moving towards one explanation may require backtracking the steps taken thus far – which may be impossible due to strict directionality of change imposed on relevant features – to arrive at a different, equally suitable counterfactual. Such a *loss of opportunity* can be measured by (a decrease in) the proportion of counterfactuals reachable after taking a step without the need of backtracking, which can be quantified by the degree of change in *path directionality* (vectors) or *vertex inaccessibility* (graphs).

**Choice Complexity** encapsulates the influence of explainees’ decisions to follow a specific counterfactual path on the availability of diverse alternative explanations. It can be understood as *loss of opportunity* accumulated along different explanatory trajectories. For example, among otherwise equivalent paths, following those whose *branching is delayed* reduces early commitment to a particular set of explanations. It can be measured by

the distance (or number of steps and their magnitude) between the factual data point and the earliest consequential point of *counterfactual path divergence*.

To illustrate the benefits of navigating counterfactuals through the lens of explanatory multiverse, consider an individual who is currently ineligible for a loan but who can follow different sets of actions to eventually receive it. Choosing one of these paths may preclude others, e.g., getting a full time job is incompatible with pursuing higher education – a scenario captured by *loss of opportunity*. Implementing the individual actions that are the most universal, thus shared across many paths to a successful loan application, allows to delay the funnelling towards specific sequences of actions – a benefit of accounting for *choice complexity*. In general, the landscape of available paths can be more easily navigated by taking actions that do not limit explainees’ choices – a prime example of *agency*. To capture these desiderata we propose a novel all-in-one metric, called *opportunity potential*, and formalise it for the vector and graph interpretations of explanatory multiverse respectively in Sections 3 and 4. It quantifies the geometrical alignment of one path with respect to another, implicitly encapsulating all of the above properties as demonstrated by the experiments reported in Section 5. Notably, we can strive for all of these desiderata simultaneously, weighting some in favour of others if necessary, which we explore further in Section 6.

## 3 Vector Space Interpretation

It should be clear by now that offering each admissible counterfactual as an independent sequence of steps and ordering these explanations purely based on their overall length fails to fully capture some fundamental, human-centred properties, e.g., agency. We must therefore seek strategies to compare the geometry of each counterfactual path, but such a task comes with challenges of its own.

**Comparing Journeys of Varying Length** Counterfactual paths may differ in their overall length, number of steps, individual magnitude thereof and the like. For example, juxtapose paths B and F in Figure 1. The former is composed of fewer steps and is much shorter than the latter, making the direct geometrical comparison via their original components infeasible – we could only do so up to the number of steps of the shorter of the two paths (assuming that these steps themselves are of similar length). We address this challenge by comparing counterfactual journeys through their normalised relative sections.

Given two paths  $Z^{[a]} \in \mathbb{R}^{m \times n_1}$  and  $Z^{[b]} \in \mathbb{R}^{m \times n_2}$  differing in their number of steps, i.e.,  $n_1 \neq n_2$ , we encode them with an equal number of vectors  $o$  such that  $\bar{Z}^{[a]}, \bar{Z}^{[b]} \in \mathbb{R}^{m \times o}$  are normalised journeys. To this end, we define a function

$$c_L(Z) = \sum_{i=1}^n \|z_i\|_2$$

that provides us with the total length of a counterfactual path  $Z \in \mathbb{R}^{m \times n}$ . We then select the number of steps  $o$  into which we partition each journey – these serve as comparison points

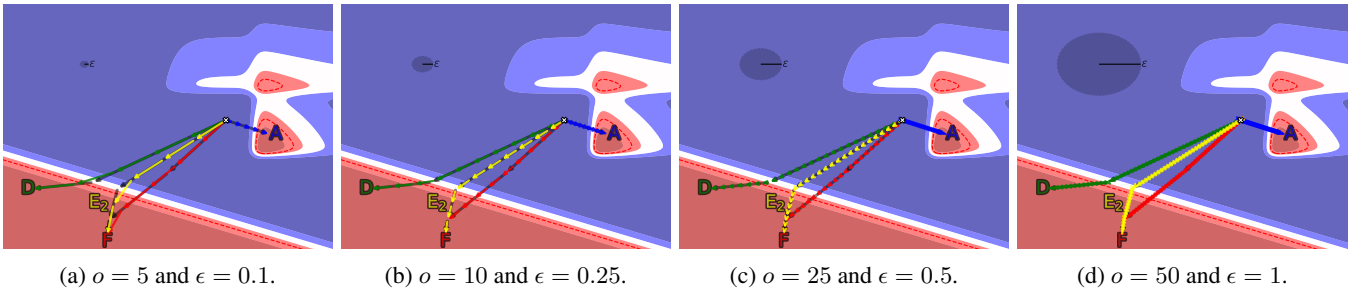


Figure 2: Demonstration of how the number of vectors  $o$  into which a path is split and the branching (i.e., divergence) threshold  $\epsilon$  affect counterfactual trajectories and branching points. These parameters must be carefully selected, which may require domain knowledge and familiarity with the underlying data; e.g., if  $\epsilon \geq 1$ , paths E<sub>2</sub> and F are not considered to diverge at any point.

for paths of differing length. Therefore, the  $j^{\text{th}}$  step  $\bar{z}_j$  of a *normalised* counterfactual journey  $\bar{Z} \in \mathbb{R}^{m \times o}$  is

$$\bar{z}_j = \sum_{i=1}^o \delta_{z_i} \left( \frac{j}{o} c_L(Z) - \sum_{l=1}^i \|z_l\|_2 \right) z_i,$$

where

$$\delta_{z_i}(\zeta) = \begin{cases} 0 & \text{if } \zeta \leq 0 \\ \frac{\zeta}{\|z_i\|_2} & \text{if } 0 < \zeta \leq \|z_i\|_2 \\ 1 & \text{otherwise.} \end{cases}$$

This procedure – demonstrated in Figure 2 above and codified by Algorithm 1 given in Appendix A – allows us to directly compare  $\bar{Z}$  with any other path normalised to the same number of steps  $o$ .

**Identifying Branching Points** We can calculate the proximity between two counterfactual paths  $\bar{Z}^{[a]}, \bar{Z}^{[b]} \in \mathbb{R}^{m \times o}$  at all points along  $\bar{Z}^{[a]}$ , therefore find the location of their divergence. To this end, we compute the minimum distance between the path  $\bar{Z}^{[b]}$  and the  $i^{\text{th}}$  point  $\bar{z}_i^{[a]}$  on the path  $\bar{Z}^{[a]}$  with

$$\bar{z}_i^{[a|b]} = d_S(\bar{Z}^{[b]} - z_i^{[a]} \mathbf{1}_o^T),$$

where

$$d_S(Z) = \min_{1 \leq j \leq o} \|z_j\|_2 = \min_{1 \leq j \leq o} \sqrt{\sum_{i=1}^m |z_{i,j}|^2}$$

and  $\mathbf{1}_o^T = [1 \ \dots \ 1]$  such that  $|\mathbf{1}_o| = o$ . Next, we define a *branching threshold*  $\epsilon > 0$  such that two paths are considered to have separated at a *divergence point*  $o^*$  where  $\bar{z}_i^{[a|b]}$  first exceeds the threshold  $\epsilon$ , i.e.,

$$o^* = \min(i) \quad \text{s.t.} \quad \bar{z}_i^{[a|b]} > \epsilon.$$

We can then denote the proportion along the journey  $\bar{Z}^{[a]}$  before it branches away from  $\bar{Z}^{[b]}$  as  $\frac{o^*-1}{o}$ . This procedure is demonstrated in Figure 2 and captured by Algorithm 2 given in Appendix A.

**Direction Difference Between Paths** After normalising two counterfactual paths to have the same number of steps, i.e.,  $\bar{Z}^{[a]}, \bar{Z}^{[b]} \in \mathbb{R}^{m \times o}$ , we can compute direction difference

between them. Popular distance metrics, e.g., the Euclidean norm, can be adapted to this end:

$$\begin{aligned} d_E(\bar{Z}^{[a]}, \bar{Z}^{[b]}) &= \sum_{j=1}^o w_j \|\bar{z}_{i,j}^{[a]} - \bar{z}_{i,j}^{[b]}\|_2 \\ &= \sum_{j=1}^o w_j \sqrt{\sum_{i=1}^m (\bar{z}_{i,j}^{[a]} - \bar{z}_{i,j}^{[b]})^2}, \end{aligned}$$

where  $d_E : Z \times Z \mapsto \mathbb{R}^+$  and the weight vector  $w$ , with  $|w| = o$ , is as outlined in Section 2.2.  $d_E$  therefore offers a measure of directional separation between two journeys such that  $d_E(\bar{Z}^{[a]}, \bar{Z}^{[b]}) = 0 \implies \bar{Z}^{[a]} \equiv \bar{Z}^{[b]}$ , and  $d_E(\bar{Z}^{[a]}, \bar{Z}^{[b]}) < d_E(\bar{Z}^{[a]}, \bar{Z}^{[c]})$  implies that  $\bar{Z}^{[a]}$  is more similar to  $\bar{Z}^{[b]}$  than to  $\bar{Z}^{[c]}$ .

**Measuring Opportunity Potential** To measure how much following a path towards one counterfactual contributes to reaching another counterfactual point we propose a novel spatially-aware metric called *opportunity potential* and denoted by  $l_{a,b}$ . It answers the question: ‘‘How close can I get from  $\hat{x}$  to  $\tilde{x}_a$  (reference path) while at the same time getting closer to  $\tilde{x}_b$  (comparison path)?’’ To this end, the metric quantifies the fraction of the reference path  $z_a$  – which we assume here to be an optimal path between  $\hat{x}$  and  $\tilde{x}_a$  – that contributes to reaching the comparison path  $z_b$ , which process is demonstrated in Figure 3. Assuming a continuous metric space, the optimal path between a factual point  $\hat{x}$  and a counterfactual instance  $\tilde{x}_a$  is given by the direct (shortest) vector linking the two:  $z_a = \tilde{x}_a - \hat{x}$ . To compute the metric we first identify the vector orthogonal to  $z_a$  that intersects with  $\tilde{x}_b$ . We find the point of intersection between this vector and  $z_a$ , and denote the difference between the intersection and the factual as  $u_{a,b}$ . The metric is therefore

$$l_{a,b} = \min \left( \frac{\|u_{a,b}\|}{\|z_a\|}, 1 \right).$$

To locate the intersection point, we parameterise the line between  $\hat{x}$  and  $\tilde{x}_a$  as

$$g(l) = (1-l)\hat{x} + l\tilde{x}_a - \tilde{x}_b,$$

and find the closest point along this line to  $\tilde{x}_b$ , i.e., the value of  $l$  that minimises  $\|g(l)\|^2$ , which is given by  $l = -\frac{z_a \cdot z_b}{z_a \cdot z_a}$



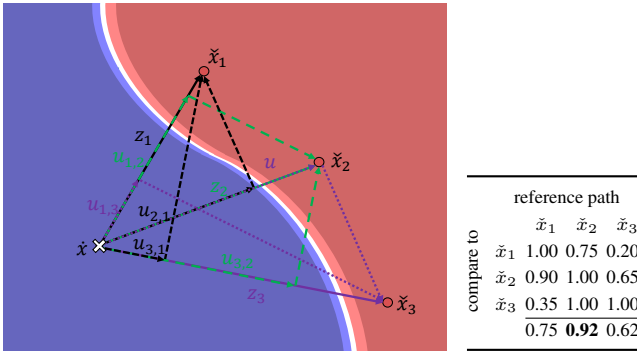


Figure 3: Visual depiction of calculating *opportunity potential* (left) and its example values (right) for vector spaces. Each element  $l_{a,b}$  of the metric table conveys how far along the reference counterfactual path from  $\hat{x}$  to  $\tilde{x}_a$  we can travel while still getting closer – albeit in a possibly sub-optimal way – to another path between  $\hat{x}$  and  $\tilde{x}_b$ ; the bottom line captures the overall opportunity potential of a path in relation to all the other paths under consideration. In this case the paths are assumed to be standalone direct vectors between the factual data point and counterfactual instances. For example, if travelling along  $z_1$  from  $\hat{x}$  to  $\tilde{x}_1$ , we can move toward the target ( $\tilde{x}_1$ ) and at the same time get closer to  $\tilde{x}_2$ ; on the other hand, travelling the same path allows us to only contribute to a small fraction of the  $\tilde{x}_3$  path, thus  $l_{1,2} > l_{1,3}$ .

(the proof is given in Appendix B). Therefore, we can reformulate the metric as

$$l_{a,b} = \begin{cases} 0 & \text{if } l < 0 \\ l & \text{if } l \in [0, 1] \\ 1 & \text{otherwise.} \end{cases}$$

The metric calculation process is formalised in Algorithm 3 given in Appendix A. If the optimal path is composed of a *series* of vectors  $Z^{[a]}$  as opposed to a single vector, we can apply the metric calculation procedure intended for graphs, which is outlined in Section 4, instead of Algorithm 3.

#### 4 Directed Graph Interpretation

Applying changes to one’s situation to achieve the desired outcome is an inherently continuous and incremental process (Barocas, Selbst, and Raghavan 2020). Given the extended period of time that it can span, this process may fail or be abandoned, e.g., due to an unexpected change in circumstances that invalidates the original plan, hence it may require devising alternative routes to the envisaged outcome. However, some of the actions taken thus far may make the adaptation to the new situation difficult or even impossible, prompting us to consider the loss of opportunity resulting from counterfactual path branching. To this end, explanatory multiverse extends the concept of counterfactual paths by accounting for uni-directional changes of features that reflect their monotonicity (as well as immutability) and recognising feature tweaks that cannot be undone. Our directed graph implementation – see Algorithm 4 in Appendix C – builds upon FACE (Poyiadzi et al. 2020) by extending its

$k$ -nearest neighbours ( $k$ -NN) approach that generates counterfactuals with the shortest path algorithm (Dijkstra 1959).

**Path Branching** Let  $r_i$  denote the *branching factor* of a node  $v_i$ , and  $r_{1,n}$  be the branching factor of a path  $E_{1,n}$  between nodes  $v_1$  and  $v_n$  consisting of  $n$  steps.  $r_i$  can be defined as the *average of the shortest distance* from a vertex  $v_i$  to each accessible node of the counterfactual class, or of all alternative classes for multi-class classification; its formulation depends on the data set and problem domain (a specific example is provided later in this section). Since there may be an overwhelmingly large number of accessible counterfactual instances (nodes), we can reduce the number of candidate points by introducing diversity criteria, e.g., (absolute) feature value difference, thus considering only a few representative counterfactuals.  $r_{1,n}$  is defined as the average of individual branching factors  $r_i$  corresponding to vertices  $v_i$  that are travelled through when following the edges  $e_{i,i+1}$  of the counterfactual path  $E_{1,n}$ , and computed as

$$r_{1,n} = \frac{1}{n-2} \sum_{i=1}^{n-1} r_i.$$

The first and last nodes are excluded since the former is shared among all the paths and we stop exploring beyond the latter. To account for choice complexity, we can introduce a discount factor  $\gamma > 0$  that allows us to reward ( $\gamma > 1$ ) or penalise ( $\gamma < 1$ ) branching in the early stages of a path, i.e.,

$$r_{1,n} = \frac{1}{n-2} \sum_{i=1}^{n-1} \gamma^{i-1} r_i.$$

**Constraining Feature Changes** Our directed graph approach accounts for feature monotonicity to capture uni-directional changes of relevant attribute values. For some data domains, however, imposing such a strict assumption may be too restrictive and yield no viable explanations, as is the case in our next example – path-based counterfactuals for the MNIST data set of handwritten digits. Here, the explanations capture (step-by-step) transitions between different digits, which process is realised through *addition* of individual pixels; the plausibility of such paths is enforced by composing them exclusively of instances observed before (and stored in a dedicated data set). As noted above, such a restrictive setup yields no viable counterfactual paths, which prompts us to relax the feature monotonicity constraint by allowing pixels to also be removed; however, we specify this action to be  $\lambda$  times more difficult than adding pixels, where  $\lambda > 0$  is a penalty term. This formalisation simulates scenarios where backtracking steps of a counterfactual path is undesirable, which in the case of MNIST can be viewed as removing pixels that are already in an image (whether pre-existing or added during recourse). The corresponding distance between two nodes  $v_a$  and  $v_b$  can be defined as

$$d_\lambda(v_a, v_b) = \sqrt{\sum_{i=1}^m (\phi_\lambda(v_{a,i}, v_{b,i})(v_{a,i} - v_{b,i}))^2},$$

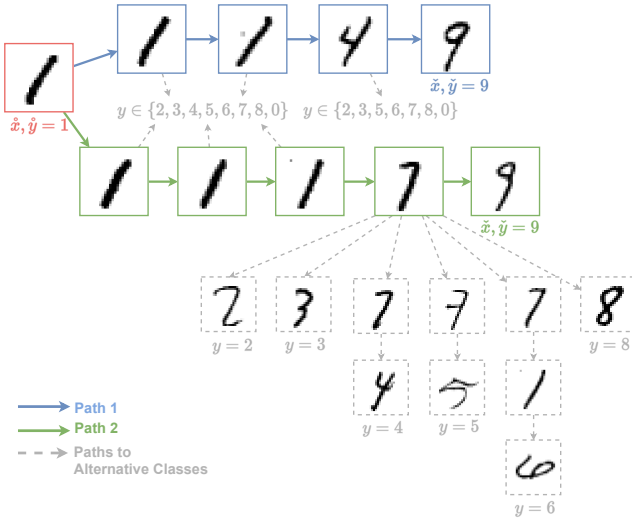


Figure 4: Example counterfactual journeys identified in the MNIST data set of handwritten digits. Paths 1 (blue) and 2 (green) are counterfactual explanations for an instance  $\hat{x}$  classified as digit 1 ( $\hat{y} = 1$ ) with the desired counterfactual class being digit 9 ( $\tilde{y} = 9$ ). Paths leading to alternative counterfactual instances of classes other than 9, i.e.,  $y \in \mathcal{Y} \setminus (1, 9)$ , are also possible (shown in grey). Path 1 is shorter than Path 2 at the expense of explainees’ agency, which is reflected by the *opportunity potential* score of 0.38 versus 0.41; therefore, switching to alternative paths that lead to different classes while travelling along Path 1 is more difficult, i.e., more costly in terms of distance.

where  $v_{a,i}$  is the  $i^{\text{th}}$  ( $1 \leq i \leq m$ ) feature of the instance  $x_a$  represented by the node  $v_a$  and

$$\phi_\lambda(v_{a,i}, v_{b,i}) = \begin{cases} -\lambda & \text{if } v_{a,i} - v_{b,i} < 0 \\ 1 & \text{otherwise.} \end{cases}$$

We apply Algorithm 4 (given in Appendix C) with  $k = 20$  using  $d_\lambda$  as the distance function, setting  $\lambda = 1.1$ . Figure 4 shows example counterfactual paths starting at  $f(\hat{x}) = 1$  and terminating at  $f(\tilde{x}) = 9$ . The branching factor of a node  $v_i$  representing a digit image is computed as  $r_i = -\log(c(v_i))$  where

$$c(v_i) = \frac{1}{|\mathcal{Y}'|} \sum_{y \in \mathcal{Y}'} \sum_{e_{m,n} \in E_{i,z}} d_\lambda(v_m, v_n) \quad \text{s.t. } f(v_z) = y.$$

Here,  $\mathcal{Y}' \equiv \mathcal{Y} \setminus (\hat{y}, \tilde{y})$ , i.e., we exclude the factual and counterfactual classes;  $E_{i,z}$  is the shortest path from  $v_i$  to all nodes  $v_z$  that represent alternative counterfactual instances, i.e.,  $f(v_z) \in \mathcal{Y}'$ . The path length indicates the number of pixels changed when transforming a factual data point into a counterfactual instance. Branching factor of a path can be interpreted as the ease of switching to alternative paths. A high branching factor for a node indicates more agency and ease of switching to counterfactual paths leading to alternative explanations. A branching factor that decreases after making a step signals that the current path begins to diverge from its viable alternatives.

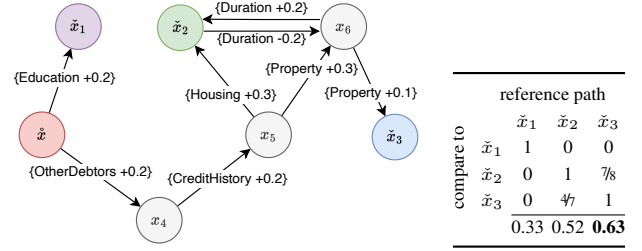


Figure 5: Visual representation of three counterfactuals –  $\tilde{x}_1$ ,  $\tilde{x}_2$  and  $\tilde{x}_3$  – for the  $\hat{x}$  instance in a loan application scenario using the (directed) graph-based explanatory multi-universe (left), and the corresponding *opportunity potential* values (right). Each element  $l_{a,b}$  of the metric table conveys how far (determined by the sum of edge weights) along the reference (shortest and optimal) counterfactual path between  $\hat{x}$  and  $\tilde{x}_a$  we can travel while still getting closer – albeit in a possibly sub-optimal way – to another path between  $\hat{x}$  and  $\tilde{x}_b$ ; the bottom line captures the overall opportunity potential of a path in relation to all the other paths under consideration. Here, the (optimal) path from  $\hat{x}$  to  $\tilde{x}_3$  maximises the explainee’s opportunity to switch to alternative paths, which is captured by the highest opportunity potential of 0.63.

**Measuring Opportunity Potential** When dealing with a (directed) graph  $G = (V, E)$ , travelling from the factual point  $\hat{x}$  to any counterfactual instance  $\tilde{x}$  requires following the graph’s edges. The *opportunity potential* metric  $l_{a,b}$  in this case quantifies how much traversing the *optimal* path to a *reference* counterfactual  $\tilde{x}_a$  contributes to approaching another counterfactual  $\tilde{x}_b$ . Here, the optimal, or shortest, path is given by a collection of edges whose summed weights are the smallest, as opposed to a direct vector connecting the factual and counterfactual instances in the feature space employed in the vector interpretation of explanatory multi-universe (see Section 3). Assume that  $V_{1,a} \subseteq V$  and  $E_{1,a} \subseteq E$  are respectively the sets of vertices and edges connecting  $\hat{x}$  to  $\tilde{x}_a$  along the optimal path, and that  $|V_{1,a}|$  denotes the number of vertices in this set, with  $v_1 \equiv \hat{x}$ ,  $v_{|V_{1,a}|} \equiv \tilde{x}_a$  and  $sum(E_{1,a})$  being the length of this path. Computing *opportunity potential* then relies on traversing the vertices of the *reference path* connecting  $\hat{x}$  to  $\tilde{x}_a$  and checking at every step whether the length of the path from this point to the alternative counterfactual  $\tilde{x}_b$  begins to increase. Such an observation signals that the reference path  $\tilde{x}_a$  starts to diverge – i.e., move away – from  $\tilde{x}_b$ , which marks the point along it where the contribution to  $\tilde{x}_b$  is the largest. This process is formalised in Algorithm 5 given in Appendix C.

A demonstration of calculating opportunity potential in a loan application scenario is given in Figure 5. This example is inspired by the German Credit data set where a user  $\hat{x}$  who is denied a loan, i.e.,  $\hat{y} = 0$ , can pursue three different counterfactual paths – to  $\tilde{x}_1$ ,  $\tilde{x}_2$  or  $\tilde{x}_3$  – to reverse this decision and receive the loan, i.e.,  $\tilde{y} = 1$ . Here, an edge of the graph corresponds to an action that affects a particular feature value. By travelling along the shortest path from  $\hat{x}$  to  $\tilde{x}_3$  – given by the  $\hat{x} \rightarrow x_4 \rightarrow x_5 \rightarrow x_6 \rightarrow \tilde{x}_3$  vertices – we

	MNIST				German Credit	
	$\hat{y} = 1, \check{y} \in \{0, 2, 3, 4, 5, 6, 7, 8\}$		$\hat{y} = 1, \check{y} = 9$		$\hat{y} = 0, \check{y} = 1$	
	distance ↓	opportunity ↑	distance ↓	opportunity ↑	distance ↓	opportunity ↑
FACE	79.33 ± 16.19	0.23 ± 0.10	79.33 ± 16.19	0.38 ± 0.19	2.16 ± 0.72	0.31 ± 0.30
GrowingSphere	<b>71.66</b> ± 34.11	0.25 ± 0.20	<b>71.66</b> ± 34.11	0.48 ± 0.34	1.68 ± 1.49	0.36 ± 0.22
Prototype	91.95 ± 47.92	0.20 ± 0.14	91.95 ± 47.92	0.53 ± 0.31	<b>1.14</b> ± 1.11	0.32 ± 0.15
FACELIFT ( $c = 5$ )	103.95 ± 16.61	0.35 ± 0.09	105.97 ± 21.05	0.59 ± 0.11	2.40 ± 0.99	0.61 ± 0.11
FACELIFT ( $c = 10$ )	110.38 ± 17.48	<b>0.36</b> ± 0.19	114.93 ± 22.73	<b>0.63</b> ± 0.09	2.54 ± 0.99	<b>0.65</b> ± 0.10

Table 1: Comparison of explainers for the MNIST and German Credit data sets based on the *distance* – measured with  $d_\lambda$  for the former and the  $L^2$ -norm for the latter – and *opportunity potential* – which quantifies the contribution of implementing an explanation to reaching its alternatives – of the most optimal counterfactual output by each explainer per queried data point. For MNIST, the factual points represent digit 1, and digit 9 is chosen to be the most desirable counterfactual class. The first group of results (left) reports statistics for when the alternative counterfactual instances are required to be of a class other than digit 9. The second group of results (right) reports statistics for when the search is restricted to counterfactuals representing digit 9. For German Credit, the target variable is binary with 0 representing *bad* and 1 representing *good* credit rating. While FACELIFT yields longer counterfactual paths on average, this sacrifice allows it to offer explainees the best opportunity potential.

can reach the target and at the same time approach  $\check{x}_2$  via the  $\hat{x} \rightarrow x_4 \rightarrow x_5$  section of this path. On the other hand, while the path to  $\hat{x}_1$  offers the smallest distance – since only one short step  $\hat{x} \rightarrow \check{x}_1$  is required – it does not contribute to reaching alternative counterfactuals. In our example, the path to  $\check{x}_3$  has the highest and the path to  $\check{x}_1$  has the lowest opportunity potential.

## 5 Experimental Evaluation

To further ground our contributions, we employ the graph-based explanatory multiverse to generate a diverse range of counterfactual paths while taking into account their spatial relation – an approach we call FACELIFT throughout our experiments. Specifically, we apply it to the German Credit (tabular, binary classification) data set (Section 5.1) and the MNIST handwritten digits (image, multi-class classification) data set (Section 5.2). We compare our method against other state-of-the-art explainers in terms of the counterfactual explanation *distance* and *opportunity potential*.

### 5.1 German Credit

We first experiment with the German Credit data set to demonstrate the increased *opportunity potential* offered by FACELIFT in the context of a loan application process.

**Data Set and Classifier** The data set consists of  $m = 20$  categorical and numerical features. The binary target variable encodes either a *good* or a *bad* credit rating, denoted by  $y = 1$  and  $y = 0$  respectively, with the former being more desirable. Following a common practice in explainability studies, we treat all the features as continuous and normalise them to the  $[0, 1]$  range, i.e.,  $\mathcal{X} = [0, 1]^m$  (Pawelczyk et al. 2022). Using 80:20 ratio we then split the data sets into two parts that we use respectively for training and evaluation. We train a simple neural network with a 50-neuron hidden layer and ReLU activation function. Given the small size of the data set, we generate recourse for all the 257 data points predicted with *bad* credit rating.

**Counterfactual Explainers** We choose three baseline explainers that can generate multiple counterfactuals for a single instance. FACE provides a sequence of existing data instances as a path to the target counterfactual based on a neighbourhood graph (Poyiadzi et al. 2020). GrowingSphere is a search-based explainer that gradually expands its search range until it finds a counterfactual instance (Laugel et al. 2023). Prototype is an explainer that encodes the data set into a latent space from which it then retrieves counterfactual examples that are close to prototypical instances of the target class (van Looveren and Klaise 2021). Since our work focuses on spatially-aware desiderata of counterfactual paths, for each factual data point we require both the counterfactual instance and a path leading to it. While FACE outputs this information by design, GrowingSphere and Prototype are not capable of it. To adapt these explainers to our experiments we employ a post-hoc path generator for counterfactual instances that is based on Binary Space Partitioning and formalised by Algorithm 6 given in Appendix E. We configure FACELIFT to identify top  $c$  closest counterfactuals – for  $c = 5$  and  $c = 10$  – and select the one with the largest opportunity potential as the explanation.

**Evaluation** To produce a diverse collection of explanations we employ a pre-existing method that filters the counterfactuals generated by each explainer such that they are at least  $\delta$  distance apart, setting  $\delta = 1$  and outputting  $c = 5$  candidate instances (Karimi et al. 2020). We use the  $L^2$ -norm to compute the distance between the factual and counterfactual instances and report the opportunity potential measured between the most optimal and all the other counterfactuals produced by an explainer.

**Results** Table 1 reports our results. The Prototype explainer generates the closest counterfactuals, but their opportunity potential is poor. FACE offers counterfactuals that are farther from the explained instance – the cost of guaranteeing a feasible path connecting the two – and it also achieves the worst opportunity potential. FACELIFT, on the



other hand, finds counterfactuals with the best opportunity potential at the expense of their distance, which is expected given the inherent trade-off between the two desiderata. This observation is further confirmed when increasing  $c = 5$  to  $c = 10$ , which enables FACELIFT to find explanations with better opportunity potential by exploring more distant explanations (i.e., with longer paths).

## 5.2 MNIST

We chose MNIST for our second set of experiments as this data set facilitates: (1) appealing and intuitive visualisations of spatially intertwined counterfactual paths as well as their direct comparison to the explanations reported by FACE (Poyiadzi et al. 2020); (2) illustration of the explanatory multiverse’s inherent capability to deal with multi-class classification, which topic is rarely explored in explainability literature (Sokol and Flach 2020b); and (3) demonstration of LIMETREE’s ability to deal with diverse data types.

**Data Set and Classifier** The data set consists of hand-written digits from 0 to 9, which are the class labels. Each image is  $28 \times 28$  pixels, and each pixel takes a value between 0 and 255, i.e., the images are greyscale. Following common practice we normalise the feature range, i.e., pixel intensity, to the  $[0, 1]$  interval, i.e.,  $\mathcal{X} = [0, 1]^m$  where  $m = 28 \times 28 = 784$  (Poyiadzi et al. 2020; van Looveren and Klaise 2021). For our experiments we randomly select 1,000 images of every digit, which yields 10,000 instances in total. Using 80:20 ratio we then split this subset into two parts that we use respectively for training and evaluation; our image classification model is a fully connected neural network. To generate counterfactual explanations, we randomly select 100 data points that represent digit 1 from the test set. We use these as our factual instances, targeting all the other classes when generating counterfactual explanations.

**Counterfactual Explainers and Evaluation** We follow the explainer setup and evaluation protocol outlined in Section 5.1, with the only deviation being the distance parameter used for explanation filtering, which for MNIST we set to  $\delta = 5$ . Also, here we experiment with two scenarios when assessing the spatial relation between multiple counterfactual instances. First, we assume that the most desirable counterfactual instances as well as the alternative counterfactuals are all from the same class – digit 9 in our experiments. This scenario captures the most prevalent counterfactual search task where the classification outcome is binary, and one result (class 9) is strictly better than the other (class 1). We further consider a largely neglected, multi-class explainability scenario where in addition to the most desirable counterfactual class we also permit a collection of alternative counterfactual classes (Sokol and Flach 2020b). In our experiments, we search for counterfactuals of class 9 for a factual instance of class 1, but we also allow for a transition to the remaining counterfactual classes  $\{0, 2, 3, 4, 5, 6, 7, 8\}$ . Examples of both these explainability scenarios are given in Appendix D.

**Results** Table 1 reports our results. In the multi-class explainability scenario the opportunity potential of the most optimal path is overall lower than in the binary explainability

setting. This is because alternative counterfactuals are more similar and closer to the optimal explanation when they are all of the same class. GrowingSphere generates the closest counterfactual explanations across the board, but it offers relatively low opportunity potential, whereas Prototype appears to balance these two desiderata; FACE yields mixed results as well. FACELIFT exhibits a similar trade-off: it achieves the highest opportunity potential at the expense of elongated paths. Its behaviour when increasing  $c = 5$  to  $c = 10$  is similar to that observed in the German Credit experiments.

## 6 Discussion

Explanatory multiverse is a novel conceptualisation of step-based counterfactual explanations (overviewed in Sections 1 and 2.1) that inherits all of their desired, spatially-unaware properties and extends them with a collection of spatially-aware desiderata that take advantage of the geometry of counterfactual paths (covered in Section 2.3). Despite being overlooked in the technical literature, such a view on counterfactual reasoning, explainability and decision-making is largely consistent with the account of these domains in philosophy, psychology and cognitive sciences (Kahneman 2014; Mueller et al. 2021). Lewis’ (1973) notion of *possible-worlds*, of which the real world is just one and with some being closer to reality (i.e., more realistic) than others (Kahneman and Varey 1990), is akin to the numerous interrelated paths connecting a factual instance with counterfactual explanations captured by our formalisation of explanatory multiverse. Specifically, it accounts for spatial and temporal contiguity, thus supports and better aligns with *mental simulation*, which is a form of automatic and elaborative (counterfactual) thinking. This process spans continuum rather than a typology and allows humans to imagine congruent links between two possible states of the world, e.g., factual and counterfactual, by unfolding a sequence of events connecting them.

Navigating the nexus of (hypothetical) possibilities through the (technical) proxy of explanatory multiverse enables structured – and possibly (interactively) guided – exploration, comparison and reasoning over (remote branches of) counterfactual explanations. By accounting for the spatial and temporal aspects of their paths – such as affinity, branching, divergence and convergence – we construct an explainability framework capable of modelling a perceptual distance between counterfactual trajectories. For example, it allows us to consider people’s tendency to first undo the changes implemented at the beginning of a process and their propensity to fall prey to the sunk cost fallacy, i.e., continuing an endeavour after the initial effort (Arkes and Blumer 1985). To the best of our knowledge, we are the first to model the geometry of explanations, thus better align ML interpretability with modes of counterfactual thinking found in humans.

Explanatory multiverse also advances the human-centred explainability agenda on multiple fronts. It comes with an inherent heuristic to deal with counterfactual multiplicity by recognising their spatial (dis)similarity, thus reducing the cognitive load required of explainees. By lowering the

choice complexity when deciding on actions to take while navigating and traversing step-based counterfactual paths, explanatory multiverse better aligns this process with iterative and interactive, dialogue-based, conversational explainability – a process that is second nature to humans (Miller 2019; Keenan and Sokol 2023). Given the ability to consider the general (geometrical) direction of representative counterfactual paths instead of their specific instantiations, which may be overwhelming due to their quantity and lack of meaningful differentiation, our conceptualisation is compatible with both the well-established *justification* as well as the more recent *decision-support* paradigms of explainable ML (Miller 2023). An additional benefit of explanatory multiverse is its ability to uncover disparity in access to counterfactual recourse – a fairness perspective; some individuals may only be offered a limited set of explanations, or none at all, if they belong to remote clusters of points, e.g., portraying a protected group that is underrepresented in the data.

The three preliminary desiderata outlined in Section 2.3 are general enough to encompass most applications of explanatory multiverse, nonetheless they are far from exhaustive; we envisage identifying more properties as we explore this concept further and apply it to specific problems. Doing so will allow us to learn about their various trade-offs, especially since we expect different data domains and modelling problems to prioritise distinct desiderata. Forgoing naïve optimisation for the shortest path in favour of a deliberate detour can benefit explainees on multiple levels as argued throughout this paper. Some of these considerations can be communicated through intuitive visualisations, making them more accessible (to a lay audience); e.g., we may plot the number of implemented changes against the proportion of counterfactual recourse opportunities that remain available at any given point.

With the current set of properties, for example, one may prefer delayed branching, which incurs small loss of opportunity early on but a large one at later stages, thus initially preserving high agency. Similarly, a small loss of opportunity early on can be accepted to facilitate delayed branching, hence reduce overall choice complexity at the expense of agency. If, in contrast, early branching is desired – e.g., one prefers a medical diagnosis route with fewer required tests – this will result in a large loss of opportunity at the beginning, thus lower agency. Additionally, certain paths may be easier to follow, i.e., preferred, due to domain-specific properties, e.g., a non-invasive medical examination, whereas others may require crossing points of no return, i.e., implementing changes that cannot be (easily) undone.

In view of the promising results offered by our experiments, streamlining and extending both of our approaches as well as implementing their variations – e.g., vector paths based on gradient methods – are the next steps, which will allow us to transition away from relatively simple scenarios and apply our tools to real-life data sets. The vector interpretation of explanatory multiverse is best suited for continuous spaces for which a sizeable and representative sample of data is available. The (directed) graph perspective, on the other hand, is more appropriate for sparse data sets with discrete attributes. Both solutions are intrinsically compatible

with multi-class counterfactuals – refer back to the MNIST example shown in Figure 4 – which explanations offer a nuanced and comprehensive explanatory perspective (Sokol and Flach 2020b). Note that an action may have multiple distinct consequences: make certain outcomes more likely (or simply possible), others less likely (or even impossible), or both at the same time; therefore, depending on the point of view, each step taken by an explainee can be interpreted as a negative or positive (counterfactual) explanation. Our solutions also facilitate *retrospective explanations* that allow to (mentally) *backtrack* steps leading to the current situation – in contrast to *prospective explanations* that prescribe actionable insights – thus answering questions such as “How did I end up here?”

## 7 Conclusion and Future Work

In this paper we introduced *explanatory multiverse*: a novel conceptualisation of counterfactual explainability that takes advantage of *geometrical relation* – affinity, branching, divergence and convergence – between paths representing the steps connecting factual and counterfactual data points. Our approach better aligns such explanations with human needs and expectations by distilling informative, intuitive and actionable insights from, otherwise overwhelming, *counterfactual multiplicity*; explanatory multiverse is also compatible with iterative and interactive explanatory protocols, which are one of the tenets of human-centred explainability.

To guide the retrieval of high-quality explanations, we formalised three *spatially-aware desiderata*: agency, loss of opportunity and choice complexity; nonetheless, this is just a preliminary and non-exhaustive set of properties, which we expect to expand as we explore explanatory multiverse further and apply it to specific data domains. In addition to foundational and theoretical contributions, we also proposed and implemented two algorithms – one based on vector spaces and the other on (directed) graphs – which we examined across three scenarios – a synthetic two-dimensional tabular data set, the MNIST handwritten digits and the German Credit data set – to demonstrate the capabilities of our approach. We then introduced a high-level, flexible evaluation metric – called *opportunity potential* – and executed experiments to numerically verify the benefit and efficacy of our approach. Our methods, the open source implementation of which is available on GitHub to promote reproducibility, are built upon state-of-the-art, step-based counterfactual explainers, such as algorithmic recourse, therefore they come equipped with all the desired, spatially-unaware properties.

By introducing and formalising explanatory multiverse we have laid the foundation necessary for further exploration of this concept. In addition to advancing our two methods, in future work we will study building *dynamical systems*, *phase spaces* and *vector fields* from (partial) sequences of observations to capture complex dynamics such as divergence, turbulence, stability and vorticity within explanatory multiverse, which appears suitable for medical data such as electronic health records. We will also look into *explanation representativeness* – i.e., identifying and grouping counterfactuals that are the most diverse and least alike – given that it is central to navigating the geometry of counterfactual

paths yet largely under-explored. Discovering (dis)similarity of counterfactuals can streamline the exploration of explanatory multiverse, whether with graphs or vectors, helping to identify pockets of highly attractive or inaccessible explanations; understanding these dependencies is also important given their *fairness ramifications* as some individuals may only have limited recourse options. Finally, we plan to investigate explanatory multiverse from a causal perspective.

### Acknowledgements

This research was conducted by the ARC Centre of Excellence for Automated Decision-Making and Society (project number CE200100005), funded by the Australian Government through the Australian Research Council. Additional support was provided by the Hasler Foundation (grant number 23082).

### Authors' Contributions

*Conceptualisation:* Kacper Sokol (lead investigator), Edward Small, Yueqing Xuan. *Methodology:* Kacper Sokol (explanatory multiverse), Edward Small (vector-based approach), Yueqing Xuan (graph-based approach). *Code development:* Edward Small (vector-based approach), Yueqing Xuan (graph-based approach). *Writing:* Kacper Sokol (explanatory multiverse), Edward Small (vector-based approach), Yueqing Xuan (graph-based approach). *Review and editing:* Kacper Sokol.

### References

- Arkes, H. R.; and Blumer, C. 1985. The psychology of sunk cost. *Organizational behavior and human decision processes*, 35(1): 124–140.
- Barocas, S.; Selbst, A. D.; and Raghavan, M. 2020. The hidden assumptions behind counterfactual explanations and principal reasons. In *Proceedings of the 2020 ACM conference on fairness, accountability, and transparency*, 80–89.
- Clark, J. N.; Small, E. A.; Keshtmand, N.; Wan, M. W. L.; Mayoral, E. F.; Werner, E.; Bourdeaux, C.; and Santos-Rodriguez, R. 2024. TraCE: Trajectory counterfactual explanation scores. In *Northern Lights Deep Learning Conference*, 36–45. PMLR.
- Dijkstra, E. W. 1959. A note on two problems in connexion with graphs. *Numerische Mathematik*, 1: 269–271.
- Downs, M.; Chu, J. L.; Yacoby, Y.; Doshi-Velez, F.; and Pan, W. 2020. CRUDS: Counterfactual recourse using disentangled subspaces. *ICML WHI*, 2020: 1–23.
- Förster, M.; Hühn, P.; Klier, M.; and Kluge, K. 2021. Capturing users' reality: A novel approach to generate coherent counterfactual explanations. In *Proceedings of the 54<sup>th</sup> Hawaii International Conference on System Sciences*.
- Hofmann, H. 1994. Statlog (German Credit Data). UCI Machine Learning Repository.
- Kahneman, D. 2014. Varieties of counterfactual thinking. In *What might have been*, 387–408. Psychology Press.
- Kahneman, D.; and Varey, C. A. 1990. Propensities and counterfactuals: The loser that almost won. *Journal of Personality and Social Psychology*, 59(6): 1101.
- Kanamori, K.; Takagi, T.; Kobayashi, K.; Ike, Y.; Uemura, K.; and Arimura, H. 2021. Ordered counterfactual explanation by mixed-integer linear optimization. In *Proceedings of the AAAI Conference on Artificial Intelligence*, volume 35, 11564–11574.
- Karimi, A.; Barthe, G.; Balle, B.; and Valera, I. 2020. Model-agnostic counterfactual explanations for consequential decisions. In *International Conference on Artificial Intelligence and Statistics*, 895–905. PMLR.
- Karimi, A.; Schölkopf, B.; and Valera, I. 2021. Algorithmic recourse: From counterfactual explanations to interventions. In *Proceedings of the 2021 ACM conference on fairness, accountability, and transparency*, 353–362.
- Keane, M. T.; Kenny, E. M.; Delaney, E.; and Smyth, B. 2021. If only we had better counterfactual explanations: Five key deficits to rectify in the evaluation of counterfactual XAI techniques. In *IJCAI*, 4466–4474.
- Keane, M. T.; and Smyth, B. 2020. Good counterfactuals and where to find them: A case-based technique for generating counterfactuals for explainable AI (XAI). In *Proceedings of the International Conference on Case-Based Reasoning*, 163–178. Springer.
- Keenan, B.; and Sokol, K. 2023. Mind the gap! Bridging explainable artificial intelligence and human understanding with Luhmann's functional theory of communication. *arXiv preprint arXiv:2302.03460*.
- Laugel, T.; Jeyasothy, A.; Lesot, M.; Marsala, C.; and Detryniecki, M. 2023. Achieving diversity in counterfactual explanations: A review and discussion. In *Proceedings of the 2023 ACM conference on fairness, accountability, and transparency*, 1859–1869.
- LeCun, Y. 1998. The MNIST database of handwritten digits.
- Lewis, D. 1973. *Counterfactuals*. Cambridge, Massachusetts: Harvard University Press.
- Miller, T. 2019. Explanation in artificial intelligence: Insights from the social sciences. *Artificial Intelligence*, 267: 1–38.
- Miller, T. 2023. Explainable AI is dead, long live explainable AI! Hypothesis-driven decision support using evaluative AI. In *Proceedings of the 2023 ACM conference on fairness, accountability, and transparency*, 333–342.
- Mothilal, R. K.; Sharma, A.; and Tan, C. 2020. Explaining machine learning classifiers through diverse counterfactual explanations. In *Proceedings of the 2020 ACM conference on fairness, accountability, and transparency*, 607–617.
- Mueller, S. T.; Veinott, E. S.; Hoffman, R. R.; Klein, G.; Alam, L.; Mamun, T.; and Clancey, W. J. 2021. Principles of explanation in human-AI systems. *AAAI 2021 Workshop on explainable agency in artificial intelligence*.
- Pawelczyk, M.; Broelemann, K.; and Kasneci, G. 2020. Learning model-agnostic counterfactual explanations for tabular data. In *Proceedings of the 2020 web conference*, 3126–3132.
- Pawelczyk, M.; Datta, T.; Van den Heuvel, J.; Kasneci, G.; and Lakkaraju, H. 2022. Probabilistically robust recourse: Navigating the trade-offs between costs and robustness in

- algorithmic recourse. In *The Eleventh International Conference on Learning Representations*.
- Poyiadzi, R.; Sokol, K.; Santos-Rodriguez, R.; De Bie, T.; and Flach, P. 2020. FACE: Feasible and actionable counterfactual explanations. In *Proceedings of the AAAI/ACM conference on AI, ethics, and society*, 344–350.
- Ramakrishnan, G.; Lee, Y. C.; and Albarghouthi, A. 2020. Synthesizing action sequences for modifying model decisions. In *Proceedings of the AAAI Conference on Artificial Intelligence*, volume 34, 5462–5469.
- Romashov, P.; Gjoreski, M.; Sokol, K.; Martinez, M. V.; and Langheinrich, M. 2022. BayCon: Model-agnostic Bayesian counterfactual generator. In *IJCAI*, 740–746.
- Russell, C. 2019. Efficient search for diverse coherent explanations. In *Proceedings of the 2019 ACM conference on fairness, accountability, and transparency*, 20–28.
- Small, E.; Xuan, Y.; Hettiachchi, D.; and Sokol, K. 2023. Helpful, misleading or confusing: How humans perceive fundamental building blocks of artificial intelligence explanations. *ACM CHI 2023 workshop on human-centered explainable AI (HCXAI)*.
- Sokol, K.; and Flach, P. 2018. Glass-Box: Explaining AI decisions with counterfactual statements through conversation with a voice-enabled virtual assistant. In *IJCAI*, 5868–5870.
- Sokol, K.; and Flach, P. 2020a. Explainability fact sheets: A framework for systematic assessment of explainable approaches. In *Proceedings of the 2020 ACM conference on fairness, accountability, and transparency*, 56–67.
- Sokol, K.; and Flach, P. 2020b. LIMETree: Consistent and faithful surrogate explanations of multiple classes. *arXiv preprint arXiv:2005.01427*.
- Sokol, K.; and Flach, P. 2020c. One explanation does not fit all. *KI-Künstliche Intelligenz*, 1–16.
- Sokol, K.; and Vogt, J. E. 2024. What does evaluation of explainable artificial intelligence actually tell us? A case for compositional and contextual validation of XAI building blocks. In *Extended Abstracts of the 2024 CHI Conference on Human Factors in Computing Systems*.
- Tolomei, G.; Silvestri, F.; Haines, A.; and Lalmas, M. 2017. Interpretable predictions of tree-based ensembles via actionable feature tweaking. In *Proceedings of the 23<sup>rd</sup> ACM SIGKDD international conference on knowledge discovery and data mining*, 465–474.
- Ustun, B.; Spangher, A.; and Liu, Y. 2019. Actionable recourse in linear classification. In *Proceedings of the 2019 ACM conference on fairness, accountability, and transparency*, 10–19.
- van Looveren, A.; and Klaise, J. 2021. Interpretable counterfactual explanations guided by prototypes. In *Proceedings of the European Conference on Machine Learning and Principles and Practice of Knowledge Discovery in Databases*, 650–665. Springer.
- Verma, S.; Boonsanong, V.; Hoang, M.; Hines, K. E.; Dickerson, J. P.; and Shah, C. 2020. Counterfactual explanations and algorithmic recourses for machine learning: A review. *arXiv preprint arXiv:2010.10596*.
- Verma, S.; Hines, K.; and Dickerson, J. P. 2022. Amortized generation of sequential algorithmic recourses for black-box models. In *Proceedings of the AAAI Conference on Artificial Intelligence*, volume 36, 8512–8519.
- Wachter, S.; Mittelstadt, B.; and Russell, C. 2017. Counterfactual explanations without opening the black box: Automated decisions and the GDPR. *Harvard Journal of Law & Technology*, 31: 841.
- Xuan, Y.; Small, E.; Sokol, K.; Hettiachchi, D.; and Sanderson, M. 2023. Can users correctly interpret machine learning explanations and simultaneously identify their limitations? *arXiv preprint arXiv:2309.08438*.

## A Vector Space Algorithms

---

Algorithm 1: Split counterfactual path  $Z$  into  $o$  vectors.

---

**Require:** counterfactual path  $Z \in \mathbb{R}^{m \times n}$ ; number of partitions  $o \in \mathbb{Z}^+$ .

**Ensure:** counterfactual path  $\bar{Z} \in \mathbb{R}^{m \times o}$  with  $o$  steps.

```

1: for  $j \leftarrow 1$ ;  $j \leftarrow j + 1$ ;  $j \leq o$  do
2:    $\beta \leftarrow \frac{j}{o} c_L(Z)$  {split path's total length}
3:    $\tau \leftarrow \mathbf{0}$ 
4:   for  $i \leftarrow 1$ ;  $i \leftarrow i + 1$ ;  $i \leq n$  do
5:     if  $\beta < 0$  then
6:       continue
7:     else if  $0 \leq \beta \leq \|z_i\|_2$  then
8:        $\tau \leftarrow \tau + \frac{\beta}{\|z_i\|_2} z_i$ 
9:     else
10:       $\tau \leftarrow \tau + z_i$ 
11:    end if
12:     $\beta \leftarrow \beta - \|z_i\|_2$ 
13:  end for
14:   $\bar{z}_j \leftarrow \tau$ 
15: end for

```

---



---

Algorithm 2: Identify branching point  $o^*$ .

---

**Require:** normalised counterfactual paths  $\bar{Z}^{[a]}, \bar{Z}^{[b]} \in \mathbb{R}^{m \times o}$ ; branching threshold  $\epsilon > 0$ .

**Ensure:** divergence point  $o^*$ .

```

1: for  $i \leftarrow 1$ ;  $i \leftarrow i + 1$ ;  $i \leq o$  do
2:   if  $\bar{z}_i^{[a|b]} > \epsilon$  then
3:      $o^* \leftarrow i$ 
4:     break
5:   end if
6: end for

```

---



---

Algorithm 3: Calculate opportunity potential given by the shared proportion of *direct* counterfactual vectors.

---

**Require:** factual instance  $\hat{x}$ ; reference counterfactual point  $\check{x}_a$ ; comparison counterfactual point  $\check{x}_b$ .

**Ensure:** opportunity potential  $l_{a,b}$  of implementing  $\check{x}_a$  as a direct, i.e., optimal, counterfactual vector with respect to  $\check{x}_b$ .

```

1:  $z_a \leftarrow \check{x}_a - \hat{x}$  {direct vector between factual and counterfactual instances}
2:  $z_b \leftarrow \check{x}_b - \hat{x}$ 
3:  $l \leftarrow -\frac{z_a \cdot z_b}{z_a \cdot z_a}$ 
4: if  $l < 0$  then
5:    $l_{a,b} \leftarrow 0$ 
6: else if  $0 < l < 1$  then
7:    $l_{a,b} \leftarrow l$ 
8: else
9:    $l_{a,b} \leftarrow 1$ 
10: end if

```

---

## B Closest Point to Parameterised Line Proof

Given three points  $x_1, x_2$  and  $x_3$ , we seek the closest point to  $x_3$  on the straight line defined by  $x_1$  and  $x_2$ . The parameterised line that connects  $x_1$  and  $x_2$  is defined as

$$f(l) = (1-l)x_1 + lx_2.$$

For  $l = 0$ ,  $f(l) = x_1$ ; and for  $l = 1$ ,  $f(l) = x_2$ . Therefore, we have an equation where the values of  $l \in [0, 1]$  represent points between  $x_1$  and  $x_2$ .

Next, we define a vector between the parameterised line and the point of interest  $x_3$  as

$$g(l) = f(l) - x_3 = (1-l)x_1 + lx_2 - x_3.$$

Our goal is to find the value of  $l$  that minimises the length of this vector such that the distance between  $x_3$  and  $f(l)$  is the shortest. The squared length of this vector is

$$\|g(l)\|^2 = (l(x_2 - x_1) + x_1 - x_3)^T \cdot (l(x_2 - x_1) + (x_1 - x_3)).$$

We represent the difference between the points of interest as vectors

$$w = x_2 - x_1 \quad \text{and} \quad u = x_1 - x_3,$$

which gives

$$\begin{aligned} \|g(l)\|^2 &= (lw + u)^T \cdot (lw + u) \\ &= l^2 \|w\|^2 + 2l(w \cdot u) + \|u\|^2. \end{aligned}$$

Finding  $\nabla \|g(l)\|^2 = 0$  gives the solution:

$$l = -\frac{w \cdot u}{w \cdot w}.$$

## C Graph Algorithms

---

Algorithm 4: Build graph-based explanatory multiverse.

---

**Require:** data set  $X$ ; probabilistic model  $\tilde{f}$ ; instance to be explained  $\hat{x}$ ; neighbours number  $k$ ; counterfactual classification threshold  $t$ .

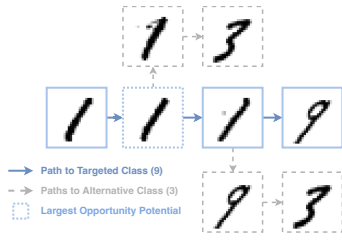
**Ensure:** directed data graph  $G = (V, E)$ ; candidate counterfactuals  $\tilde{X}$ ; branching factor of paths  $R$ .

```

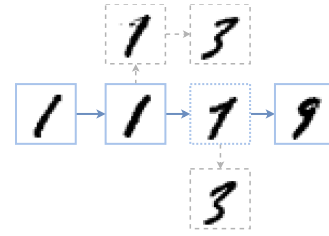
1: for every pair  $(x_i, x_j) \in X$  do {form graph edges}
2:    $e_{i,j} \leftarrow d(x_i, x_j)$  {compute distance}
3: end for
4:  $V \leftarrow X$ 
5:  $E \leftarrow \text{prune}(E, k)$  {build neighbourhood graph by keeping  $k$ -NN for each node}
6:  $x_i \equiv \hat{x}$ 
7: for  $x_j \in X$  do
8:   if  $f(x_j) \geq t$  then
9:      $\tilde{X} \leftarrow \tilde{X} \cup x_j$ 
10:     $V_{i,j}, E_{i,j} \leftarrow \text{dijkstra}(G, x_i, x_j)$  {find shortest path and the corresponding vertices}
11:     $r_{i,j} \leftarrow \text{branching}(G, E_{i,j})$ 
12:     $R \leftarrow R \cup r_{i,j}$ 
13:   end if
14: end for

```

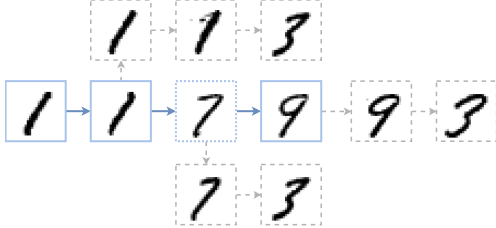
---



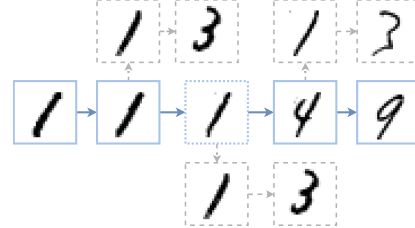
(a) The shortest path has overall *opportunity potential* of 0.14.



(b) The 2<sup>nd</sup> shortest path has overall *opportunity potential* of 0.58.



(c) The 3<sup>rd</sup> shortest path has overall *opportunity potential* of 0.62.



(d) The 4<sup>th</sup> shortest path has overall *opportunity potential* of 0.35.

Figure 6: Four different counterfactual paths targeting class 9 for the same factual instance of class 1. Due to space limitation, we only show alternative paths that lead to counterfactuals of class 3.

Algorithm 5: Calculate opportunity potential given by the shared path edges in graph-based explanatory multiverse.

**Require:** factual instance  $\hat{x}$ ; reference counterfactual point  $\tilde{x}_a$ ; comparison counterfactual point  $\tilde{x}_b$ ; directed data graph  $G = (V, E)$  from Algorithm 4.

**Ensure:** opportunity potential  $l_{a,b}$  of implementing  $\tilde{x}_a$  via its shortest, i.e., optimal, counterfactual path with respect to  $\tilde{x}_b$ .

```

1:  $V_a, E_a \leftarrow \text{dijkstra}(G, \hat{x}, \tilde{x}_a)$  {find shortest (optimal) path and the corresponding vertices}
2:  $l \leftarrow 0$ 
3: for  $i \leftarrow 2$ ;  $i \leftarrow i + 1$ ;  $i \leq |V_a|$  do
4:    $x_i \equiv v_i$  {note  $v_1 \equiv x_1 \equiv \hat{x}$  and  $v_{|V_a|} \equiv x_{|V_a|} \equiv \tilde{x}_a$ }
5:    $e_i \leftarrow \text{edge\_connecting}(v_{i-1}, v_i)$ 
6:    $V_i, E_i \leftarrow \text{dijkstra}(G, x_i, \tilde{x}_b)$ 
7:   if  $\text{sum}(E_i) \geq \text{sum}(E_{i-1})$  then
8:     break
9:   else
10:     $l \leftarrow l + e_i$ 
11:   end if
12: end for
13:  $l_{a,b} \leftarrow \frac{l}{\text{sum}(E_a)}$ 

```

## D Opportunity Potential Examples

Figure 6 shows the top four (optimal) counterfactual paths ( $\tilde{y} = 9$ ) as well as paths to an alternative class ( $\tilde{y} = 3$ ) for a single instance ( $\hat{y} = 1$ ) taken from the MNIST data set. Figure 6a depicts the shortest path, but its opportunity potential is low; past the second step the path begins to diverge from  $\tilde{y} = 3$ , i.e., digit 3 classification. The paths displayed in Figures 6b and 6c are longer but have higher opportunity potential. Figure 6d depicts the longest path whose opportunity potential is lower than that of the previous two paths, mak-

ing it sub-optimal. These examples further demonstrate the inherent trade-off between the length and opportunity potential of a counterfactual path.

## E Post-hoc Counterfactual Path Construction via Binary Space Partition

While recent research introduced numerous sequential counterfactual explainers, none of these approaches except for FACE is compatible with image data (Poyiadzi et al. 2020; Ramakrishnan, Lee, and Albarghouthi 2020; Kanamori et al. 2021; Verma, Hines, and Dickerson 2022). To adapt generic counterfactual explainers to explanatory multiverse we propose a Binary Space Partition (BSP) approach – formalised in Algorithm 6 below – that constructs counterfactual paths for a given explanation post-hoc. Such a counterfactual path is composed of a sequence of existing data instances that are located between the factual and counterfactual points. Specifically, for a given counterfactual instance we recursively partition the space between the factual and counterfactual instances at midpoints until no intermediate data points are left within these partitions or their size is smaller than a pre-defined threshold.

The counterfactual path generated by BSP is guaranteed to monotonically approach the target instance at every step. Setting the size threshold prevents partitions from becoming too small, which ensures that the counterfactual path does not consist of steps that are too close to each other to remain meaningful. On MNIST, the average number of steps in a counterfactual path generated by BSP is  $5.21 \pm 1.45$  for GrowingSphere and  $5.64 \pm 1.80$  for Prototype. For comparison, FACE is a path-based explainer that directly outputs counterfactual paths whose number of steps is  $3.37 \pm 0.69$ . Therefore, BSP performs on a par with a state-of-the-art path-based explainer.



---

Algorithm 6: Construct paths for a counterfactual explanation using Binary Space Partition.

---

**Require:** factual point  $\hat{x}$ ; counterfactual point  $\tilde{x}$ ; data set  $X$ ; partition size threshold  $\tau$ .

**Ensure:** counterfactual path  $Z$ .

```

1: function BSP( $X, x\_indices, x_a, x_b, d$ )
2:    $dist\_a \leftarrow \|X, x_a\|_2$  {compute  $L^2$  distance between
    $x_a$  and every point in  $X$ }
3:    $dist\_b \leftarrow \|X, x_b\|_2$ 
4:    $sub\_indices \leftarrow arg(dist\_a \leq d \ \&\& \ dist\_b \leq d)$ 
5:   return  $x\_indices[sub\_indices]$ 
6: function recursiveBSP( $X, x\_indices, x_i, x_j, d, \tau$ )
7:   if  $d < \tau$  then
8:      $x\_id \leftarrow random\_choice(x\_indices)$  {randomly select an instance}
9:     return  $x\_id$ 
10:  end if
11:   $mid\_point \leftarrow (x_i + x_j)/2$  {find the point splitting the space in half}
12:   $d \leftarrow d - 1$ 
13:   $partition\_l \leftarrow BSP(X, x\_indices, x_i, mid\_point, d)$ 
14:   $partition\_r \leftarrow BSP(X, x\_indices, mid\_point, x_j, d)$ 
15:  if  $partition\_l == \emptyset \ \&\& \ partition\_r == \emptyset$  then
16:     $x\_id \leftarrow random\_choice(x\_indices)$ 
17:    return  $x\_id$ 
18:  else
19:    if  $partition\_l \neq \emptyset$  then
20:       $x\_indices\_l \leftarrow recursiveBSP(X, partition\_l, x_i, mid\_point, d, \tau)$ 
21:    else
22:       $x\_indices\_l \leftarrow \emptyset$ 
23:    end if
24:    if  $partition\_r \neq \emptyset$  then
25:       $x\_indices\_r \leftarrow recursiveBSP(X, partition\_r, mid\_point, x_j, d, \tau)$ 
26:    else
27:       $x\_indices\_r \leftarrow \emptyset$ 
28:    end if
29:    end if
30:    return  $x\_indices\_l + x\_indices\_r$ 
31: function findPath( $X, \hat{x}, \tilde{x}, all\_x\_indices, \tau$ )
32:   $init\_d \leftarrow \|\tilde{x}, \hat{x}\|_2$ 
33:   $path\_points\_indices \leftarrow recursiveBSP(X, all\_x\_indices, \hat{x}, \tilde{x}, init\_d, \tau)$ 
34:   $path\_points\_indices \leftarrow sort(path\_points\_indices)$ 
   {sort indices of points based on their distance to  $\tilde{x}$ }
35:  return  $path\_points\_indices$ 
36:  $all\_x\_indices \leftarrow [0, \dots, |X|]$ 
37:  $Z \leftarrow findPath(X, \hat{x}, \tilde{x}, all\_x\_indices, \tau)$ 

```

---